Range-Stable Wireless Charging of Air-ground Robots Using Multi-Antiparallel Coils Optimized by a Hybrid Analytical-Numerical Model

Huapeng Zhao, Yuxin Zhang, Menghan Sun, Danyu Yang, Jiafeng Zhou, Zhizhang Chen, *Fellow, IEEE*, and Jun Hu, *Senior Member, IEEE*

***Abstract*—In order to accommodate robots of different heights, this paper proposes range-stable wireless charging of air-ground robots using multi-antiparallel coil (MAC). For optimal design of MAC, a new design method is developed by hybridizing analytical and numerical models. First, it is shown that the commonly used analytical model for MAC design becomes inaccurate as frequency rises. Second, a trial mutual inductance is introduced as optimization variable. From the trial mutual inductance, an MAC is designed using the analytical model. Third, the realized mutual inductance of the analytically designed MAC is computed by a numerical model to correct the error of analytical model. The difference vector $\bar{\rho}$ between the realized and optimal mutual inductances is written as a function of the trial mutual inductance, and the l_2-norm of $\bar{\rho}$ is minimized by changing the trial mutual inductance. It is shown that the resultant optimization problem is convex, and it is conveniently solved by using a local searching method. Simulation results show that the proposed design method satisfy design specification much better than conventional analytical-model-based design method. Using the proposed method, an MAC prototype is designed and fabricated, and a wireless charging system for air-ground robots is constructed and tested. Measurement results show that the efficiency of the designed MAC is maintained around 80% in the transfer range of 15 mm-55 mm, and stable voltage is obtained when charging real air-ground robots of different heights.**

***Index Terms*—Air-ground robots, convex optimization, multi-antiparallel coil, range-stable, wireless charging.**

Manuscript received xxxx, xxxx; accepted xxxx, xxxx. Date of publication xxxxxxxx xxxx, xxxx; date of current version xxxx, xxxx. This work was supported in part by the National Natural Science Foundation of China under Grant 61701087, in part by the Sichuan Science and Technology Program and in part by the Natural Science and Engineering Research Council of Canada through its Discovery Grants Program (*Corresponding Authors: Huapeng Zhao and Jiafeng Zhou*).

H. Zhao, Y. Zhang, M. Sun, D. Yang and J. Hu are with the School of Electronic Science and Engineering, University of Electronic Science and Technology of China, Chengdu 611731, China (e-mail: huapengzhao@uestc.edu.cn).

J. Zhou is with the Department of Electrical Engineering and Electronics, University of Liverpool, L69 3GJ Liverpool, U.K. (e-mail: jiafeng.zhou@liverpool.ac.uk).

Z. Chen is with the College of Physics and Information Engineering, Fuzhou University, Fujian, P. R. China 350108 and on leave from Department of Electrical and Computer Engineering, Dalhousie University, Halifax, Nova Scotia, Canada B3H 4R2, Canada (e-mail: zz.chen@ieee.org).

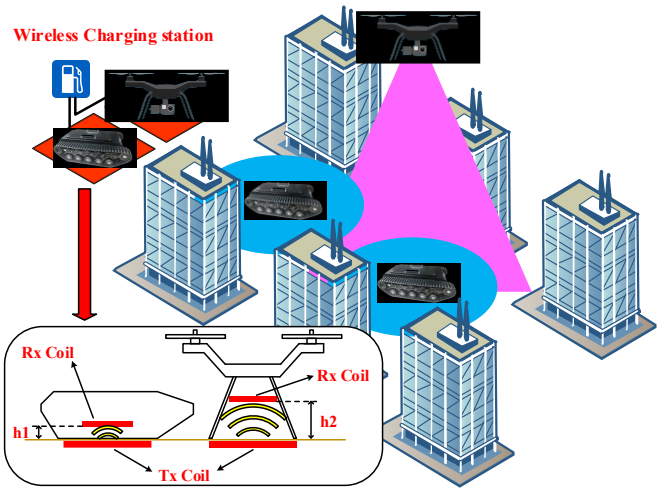

Fig. 1. Illustration of community security using air-ground robots. Wireless charging platform accommodating robots of different heights is desired.

I. Introduction

ROBOTS are indispensable to the Internet of Things (IoT). With the development of IoT, robots will be attractive in many application scenarios [1-3]. Meanwhile, more efficient and faster communication enables the collaboration of multiple robots. For example, multi-robot collaboration can be used in search and rescue [4], community security [5] and mobile base station [6, 7]. Multiple robots can share information to perceive more accurate environmental information, which is the basis for carrying out complex tasks. As shown in Fig. 1, the air-ground robot composed of unmanned aerial vehicle (UAV) and unmanned ground vehicle (UGV) is a typical example of multi-robot collaboration. UAVs are used to obtain a global view, and UGVs are used to obtain details. A shared environment map can thus be quickly built to support complex tasks [5].

Due to the limited battery capacity of a robot, it requires charging frequently and cannot work in a completely unmanned state in the case of wired charging, which greatly limits its

application. Wireless charging avoids wired charging and makes robot work in a closed loop. Therefore, wireless charging is preferred for charging air-ground robots. The UAV and UGV usually have different heights as shown in Fig. 1. Traditional wireless charging method is sensitive to separation between transmitter and receiver [8], and its transmission efficiency is not range-stable. In this case, different charging devices are needed for UAV and UGV with different heights, which increases the cost and complexity of charging platform. Range-stable wireless charging maintains efficient energy transmission even when distance changes [9, 10], which allows to wirelessly charge robots of different heights using a single transmitting coil. Therefore, it is highly desirable to develop range-stable wireless charging for air-ground robots.

This paper contributes a new design method for range-stable wireless charging of air-ground robots based on multi-antiparallel coils (MAC). The main contributions of this paper lie in the following three aspects. First, the commonly used analytical model for MAC design is revisited and it is shown that the accuracy of analytical model degrades as frequency increases. Second, a convex optimization problem combining the analytical model and a numerical model is formulated to accurately optimize MAC. With a preset trial mutual inductance, the analytical model is used to design an MAC, the mutual inductance realized by whom is computed by a numerical model. By adjusting the trial mutual inductance with a local searching method, the gap between the realized and the optimal mutual inductance is iteratively minimized. Third, using the proposed method, an MAC is designed and fabricated, and its performance is measured both before and after the Rx is installed on UAV and UGV. Measurement results show that the power efficiency of the designed coil is maintained around 80% in the transfer range of 15 mm-55 mm, which proves the effectiveness of the proposed design method. Besides, experiments show that stable load voltage can be obtained when wirelessly charging UAV and UGV of different heights, which shows the ability of wirelessly charging air-ground robots of different heights using the designed MAC.

The proposed optimization method combines the efficiency of analytical model with the accuracy of numerical model. Compared to the analytical-model-based design method, the proposed method is more accurate, especially at high frequencies where analytical model becomes inaccurate. Besides, the proposed method efficiently minimizes the error incurred by analytical model using a local searching method, and it is thus more efficient than design methods based on global searching.

The rest of this paper is organized as follows. Section II presents related work. Section III explains the proposed design method in detail. Section IV shows simulation and measurement results of a designed example, and Section V concludes this paper.

II. Related Work

Wireless charging for IoT devices recently attracts intensive research interest [11]. There are generally three paradigms for IoT wireless charging: energy harvesting, resonant beam charging, and mobile charging. Energy harvesting works like Wifi. Energy is first broadcasted by a power beacon and then harvested by IoT devices. Energy harvesting can be implemented by using Wifi or Bluetooth [12], [13]. When multiple users exist, scheduling is needed to optimize power transfer efficiency [14],[15], and beamforming can improve the quality of charging service [16]. Because energy is usually not focused in energy harvesting, it is suitable for charging low power IoT sensors scattered in a large area. Resonant beam charging (RBC) uses lasers to transfer energy, and it can focus energy in a small area [17]. Therefore, RBC is suitable for wirelessly charging high power IoT devices (e.g. vehicles [18]). For the case of multiple users, fairness and quality of charging service are taken as criterion to schedule RBC [19]-[21], and TDMA can be utilized to charge multiple users simultaneously [22]. Besides, adaptive RBC is proposed to satisfy user requirements of power level, current, and voltage [23], and a wireless energy transmission channel model is developed to investigate the maximum transfer range of RBC [24]. Though RBC can perform long-distance wireless charging, it requires line of sight link that may be interrupted by other objects. Mobile charging allows to freely establish link between transmitter and receiver, and it provides a flexible way of wireless charging [25]. Mobile charging often uses multiple mobile chargers to charge IoT devices in an area, and various algorithms are designed to optimize the coordination of multiple mobile chargers [26]-[28]. Because of their motion flexibility, UAVs are used as carriers of mobile chargers [29], and optimization algorithms searching for the shortest route of UAVs are proposed to minimize UAV power consumption [30]-[32]. Besides, mobile crowd can also be used as mobile chargers for supplying wireless energy to IoT sensors [33]. In order to maximize recharging benefit, a periodic and distributed energy supplement method is proposed [34], and the dynamic power consumption behavior of IoT sensors is learnt by the actor-critic reinforcement learning method to perform real-time dynamic scheduling of mobile charging [35]. Moreover, joint power transmission and data collection is proposed to use mobile charger as both power and communication node [36],[37].

Among the aforementioned wireless charging paradigms, mobile charging is suitable for wirelessly charging air-ground robots. Instead of moving chargers, robots can move to static charging station and get charged, as illustrated in Fig. 1. In this case, the robots can be close to the charger, and magnetic resonance coupling (MRC) can be used to link power transmitter and receiver. Traditional MRC wireless charging can only achieve high charging efficiency around a fixed distance due to the rigorous requirements of resonant condition. If the distance decreases, over-coupling will result in frequency splitting. When the distance increases, coupling will be weakened, and impedance mismatch will occur. Therefore, both increase and decrease of distance will cause MRC charging efficiency degradation [8], which means the charging efficiency is not range-stable. In order to achieve range-stable charging efficiency, various designs have been proposed, such as adaptive frequency tracking [8],[38], impedance matching

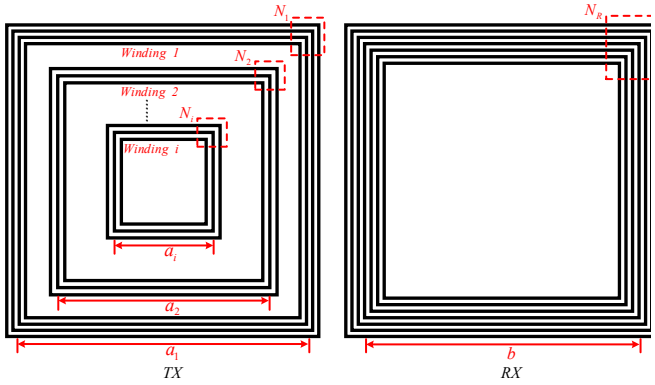

Fig. 2. Illustration of MAC: the left figure is the top view of the transmitting coil (Tx) consisting of multiple windings (each with a different number of turns), and the right figure is the top view of the receiving coil (Rx) constituted by a single winding.

[9], and switching coils [10]. However, these designs need additional circuits and control algorithm, which increases system complexity and reduces system efficiency and stability.

Recently, anti-parallel coil was proposed to suppress frequency splitting caused by over-coupling [41], and a method to determine the number of loops in anti-parallel coil is derived based on an analytical model. Literature [42] presented the concept of MAC, and used it to obtain stable power transfer efficiency, which is attractive for charging air-ground robots.

In [41] and [42], an analytical model is used to design anti-parallel coils. Nevertheless, the accuracy of the analytical model degrades as frequency increases. Considering the demand for miniaturization, high frequency wireless charging is preferred. In order to correct the error of the analytical model at high frequency, this paper proposes a design method hybridizing analytical and numerical models. In the proposed method, the design error incurred by the analytical model is efficiently minimized by solving a convex optimization problem with local searching. The design specification is thus well satisfied without a tedious and time-consuming optimization process.

III. The Proposed Design Method

A. Revisit to MAC Analytical Model

Fig. 2 illustrates MAC consisting of transmitting coil (Tx) and receiving coil (Rx). In the Tx, there are multiple windings and each of them consists of several square loops. The Rx is constituted by a single winding with a few square loops. Assume that the current direction of the outermost Tx winding is the same as the current direction of Rx. The current direction of Tx is reversed from one winding to the next, and multiple antiparallel coils is thus constructed. The parameters of MAC are explained as follows. The windings in Tx are indexed by *i*, and the total number of windings is denoted by *I*. The number of loops in the *i-th* winding is N_i, and the average side length of the square loops in the *i-th* winding is a_i. The number of loops in the Rx is N_R, and the average side length of these loops is *b*. The wireless charging efficiency of MAC is mainly determined by the total mutual inductance between Tx and Rx, which is actually the superposition of the mutual inductance between every Tx winding and Rx. The total mutual inductance is then written as follows

$$M(h)=\sum_{i=1}^{I}(-1)^{i-1}N_iM_i(h) \tag{1}$$

where M_i is the mutual inductance between all Rx loops and a single loop of the *i*-th Tx winding, and *h* is the separation between Rx an Tx. Note that central approximation is used to obtain (1), assuming that all loops of a Tx winding are located in the middle of the outermost and innermost loops of the winding. The coefficient $(-1)^{i-1}$ in (1) is due to the reversal of current direction from one Tx winding to the next. In equation (1), M_i can be computed by

$$M_i(h)=N_RM(a_i,b,h) \tag{2}$$

where $M(a_i,b,h)$ is the mutual inductance between two coaxial square loops with side lengths a_i and b, respectively. The mutual inductance between two coaxial square loops can be calculated as follows [43]

$$\begin{aligned}&M(a_i,b,h)=\\&\frac{2\mu_0}{\pi}\left[\sqrt{2(c+d)^2+h^2}+\sqrt{2(c-d)^2+h^2}-2\sqrt{2c^2+2d^2+h^2}\right.\\&+(c+d)\left[\tanh^{-1}\left(\frac{c+d}{\sqrt{2c^2+2d^2+h^2}}\right)-\tanh^{-1}\left(\frac{c+d}{\sqrt{2(c+d)^2+h^2}}\right)\right]\\&\left.+(c-d)\left[\tanh^{-1}\left(\frac{c-d}{\sqrt{2c^2+2d^2+h^2}}\right)-\tanh^{-1}\left(\frac{c-d}{\sqrt{2(c-d)^2+h^2}}\right)\right]\right]\end{aligned} \tag{3}$$

where μ_0 is the permeability of vacuum and

$$c=\frac{a_i}{2} \tag{4.1}$$

$$d=\frac{d}{2} \tag{4.2}$$

Equations (1) to (4) is the analytical model of MAC. From (1) to (4), it can be observed that the design parameters of MAC include *h*, *b*, a_i, *I*, N_R and N_i. Among these parameters, *h* is determined by the heights of robots, *b* (the size of Rx) is determined by the space left for placing the Rx on the robots, and a_1 (the average loop size of the first Tx winding) is determined by the space left for placing the Tx on the charging platform. a_i for $i=2,...I$ (the average loop sizes of the remaining Tx windings) and *I* (the total number of Tx windings) can be estimated based on the rule that spacing between neighboring windings should be sufficiently large so that each winding will contribute to the total mutual inductance differently from its neighboring windings. From (1) and (2), it can be seen that the total mutual inductance is simply scaled by N_R (the number of loops in Rx). Therefore, N_R is not a critical design parameter, and its value can be determined

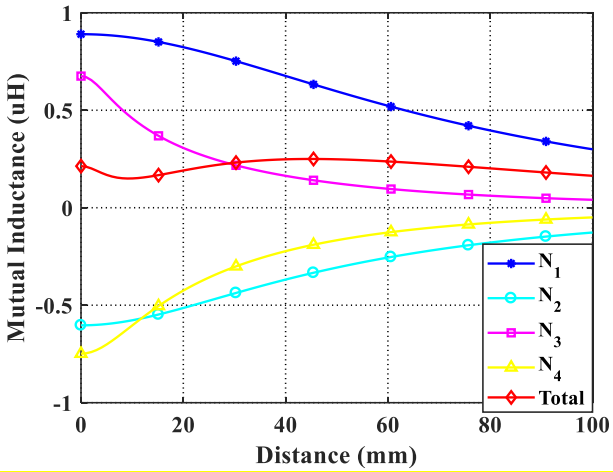

Fig. 3. Mutual inductance versus distance (computed by the analytical model).

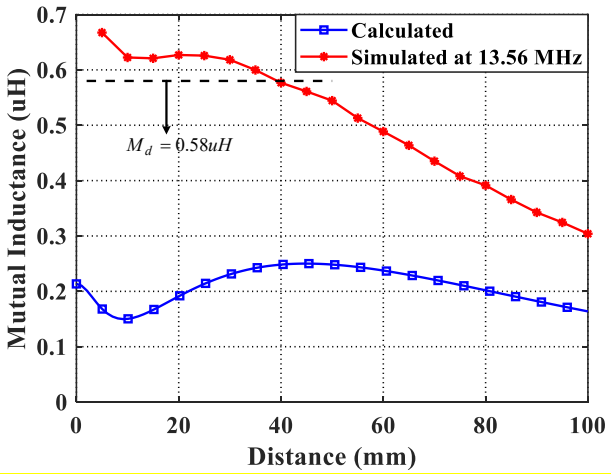

Fig. 4. Comparison between mutual inductances computed by analytical and numerical models.

empirically. Besides, from equation (1), it can be seen that N_i (the number of loops in the i-th winding) determines how the contributions of Tx windings are combined. Therefore, N_i is a critical design parameter. In this paper, it is assumed that h, b, a_i, I and N_R are fixed, and N_i is optimized to achieve range stable wireless charging.

The analytical model presented in (1) to (4) can be used to conveniently compute mutual inductance. Fig. 3 presents the mutual inductance computed by using the analytical model. Both total mutual inductance and the contribution of every winding are shown. In Fig. 3, the horizontal axis is the separation between Tx and Rx. From Fig. 3, it can be seen that the total mutual inductance changes much more slowly than the mutual inductance between Rx and a single Tx winding, which means the MAC can provides range-stable wireless charging efficiency. Although the analytical model allows to compute the mutual inductance with negligible time cost, it only considers the static inductive coupling effect and can cause design error for magnetic resonance coupling at high frequency where time harmonic electromagnetic effects are involved. Fig. 4 compares the total mutual inductances computed by the analytical model and by a numerical model based on finite element method. In the numerical model, the frequency of operation is 13.56 MHz. The numerical model solves time-harmonic Maxwell's equations by using the finite element method, and it can provide accurate computation of mutual inductance at high frequency. From Fig. 4, it can be observed that the results of analytical model deviates from those of numerical model. The cause of this deviation is further investigated by performing frequency sweep of the mutual inductance using the numerical model. Fig. 5 presents total mutual inductance versus frequency. The inset of Fig. 5 shows that the mutual inductance is around 0.25 uH when the frequency is 1 MHz, which agrees with the result of analytical model. The mutual inductance slowly increases until frequency reaches 25 MHz, where a sharp change of mutual inductance occurs. After 25 MHz, the mutual inductance becomes negative, which means the coupling between Tx and Rx is capacitive for frequency above 25 MHz. From the inset

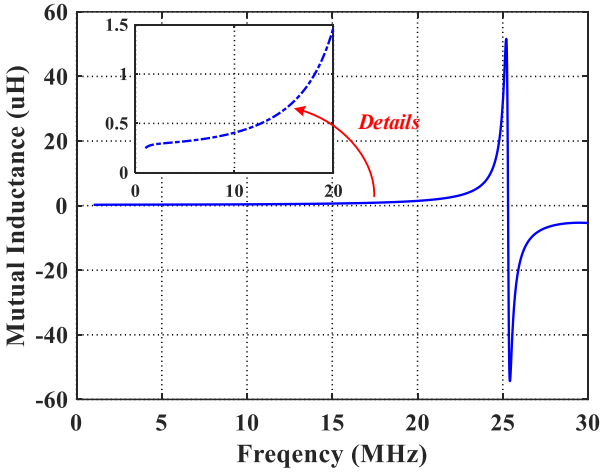

Fig. 5. Total mutual inductance versus frequency computed by the numerical model (h=50 mm).

of Fig. 5, it can be seen that as frequency goes closer to 25 MHz, the change of mutual inductance becomes more and more drastic. Such kind of frequency-domain behavior of mutual inductance is caused by the high frequency resonance of the MAC around 25 MHz. This frequency-domain behavior is not considered in the analytical model, which results in inaccuracy at high frequency.

B. Optimization by Hybrid Analytical-Numerical Model

From the previous section, it is known that the analytical model is inaccurate at high frequency. Although numerical model is accurate, it is computation intensive and the number of numerical simulations should be as few as possible during optimization process. In order to reduce the number of numerical simulations, a new optimization method is developed by hybridizing analytical and numerical models. The proposed method consists of the following two steps.

First, the analytical model is utilized to design a range stable MAC as follows. It is known that maximum charging efficiency can be obtained by optimizing the mutual inductance [44]. The optimal mutual inductance that maximizes the charging efficiency can be computed by [42]

$$M_{optimal}=\frac{\sqrt{R_S R_L}}{\omega_0} \tag{5}$$

where R_S is the source resistance, R_L is the load resistance and ω_0 is the resonant angular frequency. In order to achieve range-stable charging efficiency, the mutual inductance should be around $M_{optimal}$ in the range of interest. However, considering the inaccuracy of the analytical model, a trial mutual inductance M_d, instead of $M_{optimal}$, is taken as the targeted mutual inductance of the analytical model. Assume the range of interest is $[h_1,h_2]$. N_t-1 sampling points are uniformly selected in the range of interest. Based on point matching, the total mutual inductance at the sampling points is enforced to be equal to the trial mutual inductance M_d, and the following equation can be obtained at the n-th sampling point

$$\sum_{i=1}^{I}(-1)^{i-1}N_i M_i(h_n)=M_d \tag{6}$$

Traversing all $I-1$ sampling points, the following matrix equation can be established:

$$\bar{\bar{K}}\bar{N}=\bar{V} \tag{7}$$

where $\bar{N}$ is a column vector consisting of N_i, $\bar{V}$ is a column vector with all elements equal to M_d, $\bar{\bar{K}}$ is a matrix with $I-1$ rows and I columns, and its (n,i)-th element is

$$K_{(n,i)}=(-1)^{i-1}M_i(h_n) \tag{8}$$

By solving (7), the number of loops N_i for every winding in Tx can be obtained, and the total mutual inductance will be around M_d in the range of $[h_1,h_2]$. It should be mentioned that the matrix equation in (7) is purposely made underdetermined. This is because the underdetermined matrix equation has infinite number of solutions, from which one can choose a solution that is physically meaningful. In the paper, the underdetermined matrix equation is solved by the combination of its special and general solutions. Namely, the solution of (7) is found by

$$\bar{N}=\sum_{l=1}^{L}\alpha_l\bar{v}_l+M_d\bar{P} \tag{9}$$

where $\bar{v}_l$ is the l-th right singular vector of matrix $\bar{\bar{K}}$, α_l is the combination coefficient of $\bar{v}_l$, L is the total number of right singular vectors of $\bar{\bar{K}}$, $\bar{P}=\bar{\bar{K}}^{\dagger}\bar{U}$, $\bar{\bar{K}}^{\dagger}$ is the pseudo inverse of $\bar{\bar{K}}$, and $\bar{U}$ is a column vector with all its elements equal to one.

Second, a numerical model is constructed based on the number of loops N_i determined by the analytical model, with the separation between Tx and Rx uniformly sampled in the range of $[h_1,h_2]$. The total realized mutual inductances $M_r(h_p)$ are then computed by using the numerical model, where h_p is the p-th (p=1,2,…,P) separation sample to compute total realized mutual inductance, and P is the total number of samples. Note that h_p is different from h_n in (6). The former is used for checking the performance of the designed MAC, and the latter is used to solve $\bar{N}$. The total realized mutual inductance can be considered as the superposition of the mutual inductance between Rx and every Tx winding, namely

$$M_r(h_p)=\sum_{i=1}^{I}N_i(-1)^{i-1}M_i'(h_p) \tag{10}$$

where M_i' is the realized mutual inductance between the i-th Tx winding and Rx. Varying p from 1 to P, the following matrix equation is obtained from (10)

$$\bar{M}_r=\bar{\bar{K}}'\bar{N} \tag{11}$$

where $\bar{M}_r$ is a column vector consisting of $M_r(h_p)$ (p=1,2,…,P), and the (p,i)-th element of $\bar{\bar{K}}'$ is

$$K_{(p,i)}=(-1)^{i-1}M_i'(h_p) \tag{12}$$

Substituting (9) into (11), one can have

$$\bar{M}_r=\sum_{l=1}^{L}\alpha_l\bar{S}_l+M_d\bar{T} \tag{13}$$

where

$$\bar{S}_l=\bar{\bar{K}}'\bar{v}_l \tag{14.1}$$

$$\bar{T}=\bar{\bar{K}}'\bar{P} \tag{14.2}$$

In order to optimize $\bar{M}_r$, the following error vector $\bar{\rho}$ is defined

$$\bar{\rho}=\bar{M}_r-\bar{M}_o \tag{15}$$

where $\bar{M}_o$ is a column vector with all elements equal to $M_{optimal}$. Equations (13) and (14) indicate that $\bar{M}_r$ is a function of α_l and M_d. An optimization problem is then formulated as

$$\min_{\alpha_l,M_d}\|\bar{\rho}\|_2^2 \tag{16.1}$$

$$\text{subject to } 0<M_d\le M_u \tag{16.2}$$

where M_u is the upper bound of M_d. Substituting (13) into (15), $\|\bar{\rho}\|_2^2$ can be expressed by equation (17) shown at the bottom of this page. From (17), it can be seen that $\|\bar{\rho}\|_2^2$ is a quadratic function of M_d and α_l. Therefore, the optimization problem in (17) is a convex problem that can be efficiently solved by a local optimization method.

Although (17) shows the convexity of the optimization problem in (16), it cannot be used to solve (16). This is because the computation of $\bar{S}_l$ and $\bar{T}$ in (17) requires the knowledge

$$\begin{aligned}\|\bar{\rho}\|_2^2&=\left[\sum_{l=1}^{L}\alpha_l\bar{S}_l+M_d\bar{T}-\bar{M}_o\right]^T\left[\sum_{l=1}^{L}\alpha_l\bar{S}_l+M_d\bar{T}-\bar{M}_o\right]\\&=M_d^2\bar{T}^T\bar{T}+M_d\left\{\bar{T}^T\left[\sum_{l=1}^{L}\alpha_l\bar{S}_l-\bar{M}_{optimal}\right]+\left[\sum_{l=1}^{L}\alpha_l\bar{S}_l-\bar{M}_{optimal}\right]^T\bar{T}\right\}+\sum_{l=1}^{L}\sum_{t=1}^{L}\alpha_l\alpha_t\bar{S}_l^T\bar{S}_t-\sum_{l=1}^{L}\alpha_l\bar{S}_l^T\bar{M}_o-\sum_{l=1}^{L}\alpha_l\bar{M}_o^T\bar{S}_l+\bar{M}_o^T\bar{M}_o\end{aligned} \tag{17}$$

of M_i', the realized mutual inductance between Rx and a single loop of the i-th Tx winding. The total realized mutual inductance can be computed by the numerical model, but M_i' cannot be extracted from the total realized mutual inductance. Therefore, in this paper, $\bar{\rho}$ is computed using (15), where $\bar{M}_r$ is obtained by the numerical model based on finite element method, and the convex optimization problem in (16) is solved as follows. First, M_d is set to $M_{optimal}$, $\bar{N}$ is computed using (9). When computing $\bar{N}$, α_l should be determined first. Because I is small, L wont' be large and α_l can be easily determined by a quick trial and error process based on the criterion that elements of $\bar{N}$ are close to small integers. Once α_l is determined, it is fixed throughout the remaining optimization process. Second, considering the convexity of the optimization problem in (16), the performance of MAC is optimized by using the following local searching method.

1. $M_{optimal} \rightarrow M_d$; Compute $\bar{N}$ using (9); $\bar{N} \rightarrow \bar{N}_1$; Perform numerical simulations and compute $\bar{\rho}$ using (15); $\|\bar{\rho}\|_2^2 \rightarrow \varepsilon_1$.
2. (M_d +0.05$M_{optimal}$) $\rightarrow M_d$; Compute $\bar{N}$ using (9); $\bar{N} \rightarrow \bar{N}_2$; Perform numerical simulations and compute $\bar{\rho}$ using (15); $\|\bar{\rho}\|_2^2 \rightarrow \varepsilon_2$.
3. $(\varepsilon_2\text{-}\varepsilon_1) \rightarrow \varphi_2$; $\varphi_2/|\varphi_2| \rightarrow q$; $3 \rightarrow k$.
   If q<0
   $M_d \rightarrow M_d^{k-1}$.
   Else
   $M_{optimal} \rightarrow M_d^{k-1}$; $\bar{N}_1 \rightarrow \bar{N}_{k-1}$.
   End If
   -$|\varphi_2| \rightarrow \varphi_2$; $10 \rightarrow k_{\max}$.
6. If $k<k_{\max}$ and φ_{k-1} <0
   ($M_d^{k-1} - q \times 0.05 M_{optimal}$) $\rightarrow M_d$; $M_d \rightarrow M_d^k$.
   Else
   Return $\bar{N}_{k-1}$; terminate optimization.
   End If
7. Compute $\bar{N}$ using (9); Perform numerical simulations to compute $\|\bar{\rho}\|_2^2$ and the transmission coefficients between Tx and Rx for all values of h_p (p=1,2,…,P); $\|\bar{\rho}\|_2^2 \rightarrow \varepsilon_k$.
8. $(\varepsilon_k\text{-}\varepsilon_{k-1}) \rightarrow \varphi_k$;
9. If transmission coefficients for all values of h_p satisfy design requirements, return $\bar{N}$ and terminate optimization; otherwise $\bar{N} \rightarrow \bar{N}_k$, ($k$+1)$\rightarrow k$, and go to step 6.

Using the aforementioned procedures, the power transfer efficiency of MAC can be optimized. Note that the final objective of the optimization is to achieve range stable wireless charging, and hence the optimization is terminated when the transmission coefficients for all values of h_p satisfy design requirements.

TABLE I
PARAMETERS OF MAC DESIGNED USING THE PROPOSED METHOD

Parameter	Average Side Length (mm)	Number of Loops
Tx Wingding 1	200	2
Tx Wingding 2	160	1
Tx Wingding 3	110	0.5
Tx Wingding 4	80	1
Rx	100	7
Gap: 2 mm	Loop Width: 2 mm	

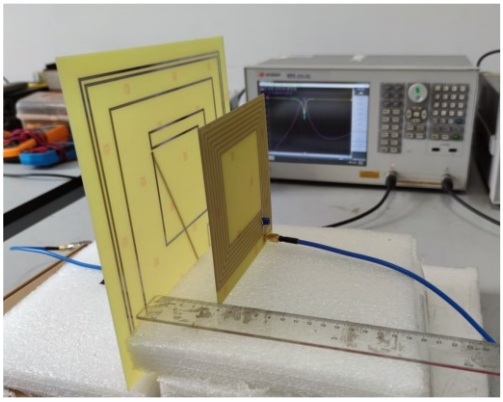

Fig. 6. Fabricated MAC and measurement setup using a vector network analyzer.

IV. RESULTS AND DISCUSSION

This section presents simulation and measurement results to prove the effectiveness of the proposed design method. First, an MAC is designed using the proposed method, and simulation and measurement results are presented to validate the design method. Second, the proposed optimization method is compared with existing MAC design methods to illustrate its advantages. Third, real UAV and UGV are used as robots, and wireless charging systems for air-ground robots are constructed. Experiments are performed to illustrate the wireless charging stability for air-ground robots with different heights.

A. Design Example of MAC

The geometrical dimensions of the MAC are determined based on the space left for placing MAC on the charging platform and air-ground robots, and their values are presented in Table I. Charging heights of the considered UAV and UGV are 50 mm and 17 mm, respectively. Because it is more difficult to obtain stable charging for small separation than for large separation, the separation range of interest is set to 2-50 mm so that stability can be guaranteed for the charging height of 17 mm. The number of Tx windings is set to four, and three separation samples are uniformly chosen as h_n to construct the matrix equation in (7). Besides, nine samples are uniformly chosen for h_p to compute $\|\bar{\rho}\|_2^2$. The resonant frequency is set to 13.56 MHz, the source and load impedances are both 50 Ω, and $M_{optimal}$ is set to 0.587uH according to (5). With the aforementioned parameters, the proposed optimization is applied. Convergence is achieved after five iterations, and the obtained number of loops are shown in Table I.

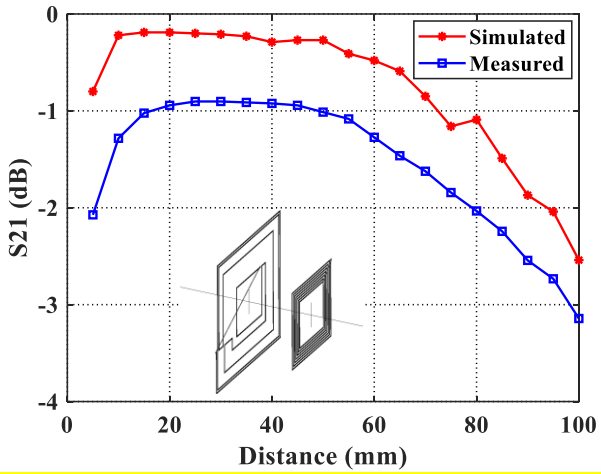

Fig. 7. The simulated and measured results of $|S_{21}|$ versus separation at 13.56 MHz.

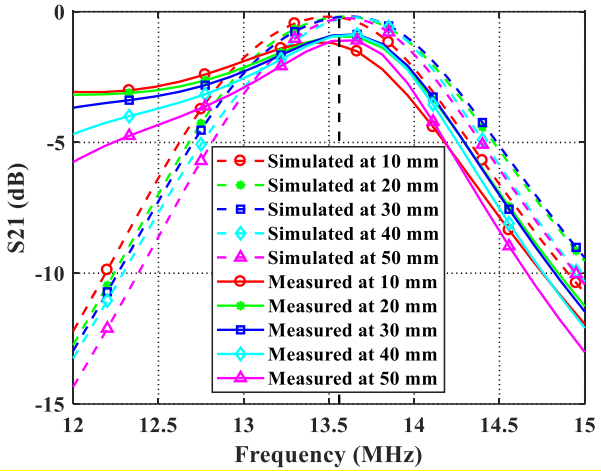

Fig. 9. The simulated and measured $|S_{21}|$ versus frequency for different separations.

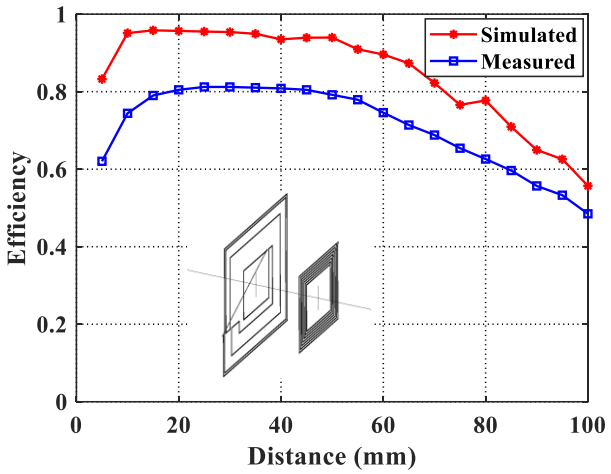

Fig. 8. The simulated and measured wireless power transfer efficiency versus separation at 13.56 MHz.

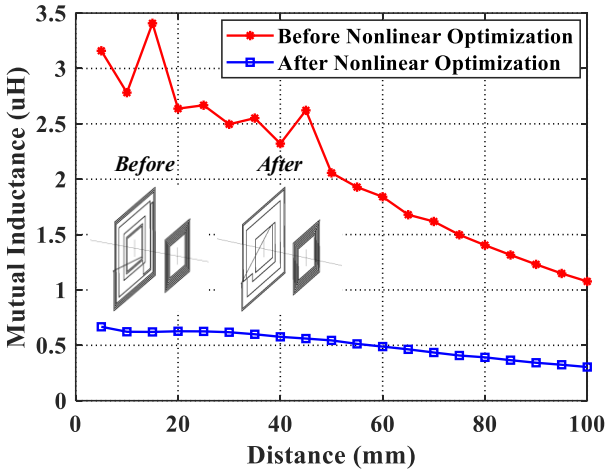

Fig. 10. The total realized mutual inductance at 13.56 MHz before and after optimization.

The designed MAC has been fabricated and measured. The fabricated MAC and the measurement setup are shown in Fig. 6. The coil is printed on 1.6 mm-thick dielectric substrate made of FR4. The measurement instrument is vector network analyzer E5061B. The simulated and measured results of $|S_{21}|$ (transmission coefficient amplitude between Tx and Rx) versus separation at 13.56 MHz are shown in Fig. 7. The measured and simulated values of $|S_{21}|$ are close to each other, and the difference between them is less than 1dB for most separation values. The measured values are always less than the simulated values, which means the difference could be due to some practical loss ignored in the simulation model. The wireless power transfer efficiency (the square of $|S_{21}|$) is shown in Fig. 8. It can be seen that the simulated efficiency can be maintained around 94% in the range of 10-50 mm, and the measured efficiency is maintained around 80% in the range of 15-55 mm. The variation of $|S_{21}|$ versus frequency at different separations is shown in Fig. 9. It can be seen that no frequency splitting occurs, and $|S_{21}|$ has a good stability at 13.56 MHz in both simulation and measurement. From the simulation and measurement results shown in Figs 7 to 9, it can be concluded that the MAC designed by using the proposed method can achieve stable power transfer efficiency versus separation between Rx and Tx.

B. Comparison with Existing MAC Design Methods

Currently, most MAC design methods are based on analytical model [41],[42]. As discussed in Section III-A, the analytical model is accurate at low frequency, but it incurs design error at high frequency, which can be corrected by using the proposed optimization method. In order to illustrate the advantages of the proposed method, it is compared with the design method based on analytical model. Fig. 10 presents the total realized mutual inductances of MACs designed based on analytical model and the proposed method. In analytical-model-based design, M_d is set to the optimal mutual inductance, and the number of loops is computed using (9). In fact, the analytical-model-based design is the initial design in the proposed design method. From Fig. 10, it can be observed that the total realized mutual inductances obtained by using analytical model deviate significantly from the optimal mutual inductance. On the other hand, after the proposed optimization process, the realized

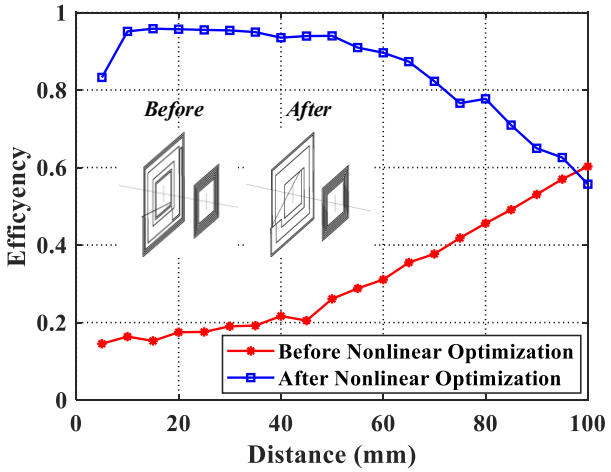

Fig. 11. The simulated efficiency at 13.56 MHz before and after optimization.

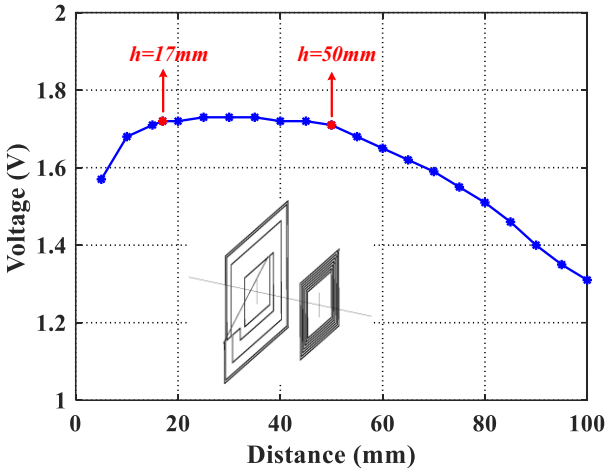

Fig. 12. The load voltage versus separation when the Rx coil is not installed.

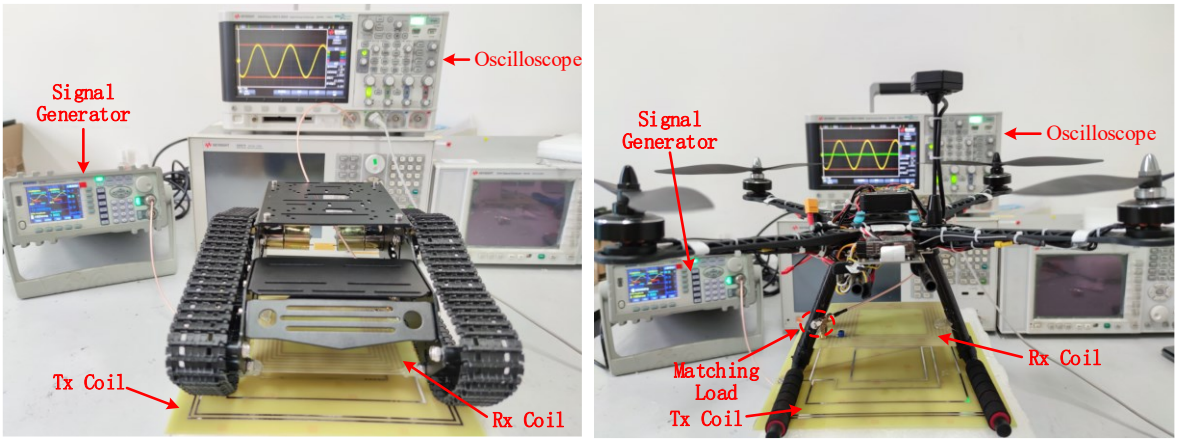

Fig. 13. The setup of air-ground robot wireless charging experiments using UGV and UAV.

TABLE II
COMPARISON BEFORE & AFTER INSTALLATION OF RX

	UGV (h=17 mm)	UAV (h=50 mm)
Before installation	1.72 V	1.71 V
After installation	1.57 V	1.64 V

mutual inductance is close to the optimal value in the range of interest. Fig. 11 presents the wireless charging efficiency of MACs designed based on analytical model and the proposed method. From Fig. 11, it can be observed that the efficiency of MAC designed using analytical model is around 20% in the range of interest, while the MAC designed using the proposed method renders more than 90% charging efficiency in the range of interest. In conclusion, by applying the proposed method, the error of analytical-model-based design is corrected, and the design target is achieved.

Another possible approach to design MAC is to utilize numerical model and global searching for the optimization of the number of loops in every Tx winding. Because global searching is much more time consuming than local searching, the design approach based on global searching will require more CPU time than the proposed local-searching-based optimization method. The advantage of global searching lies in its ability of avoiding local convergence. Considering the convexity of the optimization problem presented in (16), global convergence can be guaranteed even if local searching is applied. Therefore, it is unnecessary to perform time-consuming global searching to solve (16). Moreover, considering the essentially different application scenarios of global and local searching methods, the authors choose not to make direct CPU time comparison between global searching method and the proposed method.

C. *Wireless Charging of Air-ground Robots*

In order to verify the effectiveness of MAC for wireless charging of air-ground robots, wireless charging experiments on real UGV and UAV are designed and performed. During the experiments, a signal generator is used as Tx source and a 50 Ω resistor is used as Rx load. The output voltage of the signal generator is 2 V. The RMS value of AC voltage on the load resistor is measured by oscilloscope DSO-X 2024A, and it is used to evaluate the stability of wireless charging. In order to investigate the stability of wireless charging before and after Rx is installed on robots, the stability of the load voltage is first investigated before Rx is installed on robots. The load voltage versus separation is shown in Fig. 12. It can be seen that the changing trend of the load voltage is similar with the changing trend of efficiency shown in Fig. 8, and the voltage is around 1.7 V for both h=17 mm and h=50 mm.

The Rx and load resistor are then installed on UGV and UAV. The installation heights of Rx in UGV and UAV are 17

mm and 50 mm, respectively. The experiment setup is shown in Fig. 13. The load voltages of Rx before and after Rx is installed on robots are listed in Table II. It can be seen from Table II that the load voltage is stable versus charging height both before and after Rx is installed on robots. Besides, after the Rx is installed on robots, the load voltage slightly decreases due to the influence of the robots' body. The Rx of UAV is far away from the metal frame of UAV, so the decrease of voltage is small. On the other hand, the Rx of UGV is close to its metal frame, which results in relatively larger decrease of voltage. Therefore, the impact of metal structures in the working environment of MAC needs to be considered in practical applications, which will be investigated in future work. To sum up, the load voltage of Rx remains stable both before and after Rx is installed on robots, and the experimental results illustrate range stable charging performance when wirelessly charging air-ground robots using the designed MAC.

V. Conclusion

This paper has presented a new MAC design method for range-stable wireless charging of air-ground robots. The commonly used analytical model of MAC has been revisited, and it has been shown that the high frequency effects are ignored in the analytical model, which results in design error in analytical-model-based design method. A new optimization problem was then formulated by hybridizing the analytical model with the numerical model. The newly formulated optimization problem has been proved to be convex, and it has been efficiently solved by using a local searching method. An MAC has been designed using the proposed method, and simulation and measurement results have shown the effectiveness of the proposed design method. Moreover, comparisons between the proposed method and existing design methods have shown that the proposed method is more accurate than analytical-model-based design method, and it is more efficient than design method based on global searching. Finally, wireless charging experiments on real UGV and UAV have illustrated range stable charging ability of the designed MAC when wirelessly charging air-ground robots. Experimental results have also shown that the charging performance can be influenced by the working environment, which will be further investigated in future work.

References

[1] H. Wang, H. Zhao, W. Wu, J. Xiong, D. Ma, and J. Wei, "Deployment Algorithms of Flying Base Stations: 5G and Beyond With UAVs," IEEE Internet of Things Journal, 6, pp. 10009-10027, (2019).

[2] L. Xie, J. Xu and R. Zhang, "Throughput Maximization for UAV-Enabled Wireless Powered Communication Networks," IEEE Internet of Things Journal, 6, pp. 1690-1703, (2019).

[3] Z. Hu, S. Cong, T. Song, K. Bian, and L. Song, "AirScope: Mobile Robots Assisted Cooperative Indoor Air Quality Sensing by Distributed Deep Reinforcement Learning," IEEE Internet of Things Journal, p. 1-1.

[4] E. T. Alotaibi, S. S. Alqefari and A. Koubaa, "LSAR: Multi-UAV Collaboration for Search and Rescue Missions," IEEE Access, 7, pp. 55817-55832, (2019).

[5] J. Zhang, R. Liu, K. Yin, Z. Wang, M. Gui, and S. Chen, "Intelligent Collaborative Localization Among Air-Ground Robots for Industrial Environment Perception," IEEE T. Ind. Electron., 66, pp. 9673-9681, (2019).

[6] B. Li, Z. Fei and Y. Zhang, "UAV Communications for 5G and Beyond: Recent Advances and Future Trends," IEEE Internet of Things Journal, 6, pp. 2241-2263, (2019).

[7] X. Li, H. Yao, J. Wang, S. Wu, C. Jiang, and Y. Qian, "Rechargeable Multi-UAV Aided Seamless Coverage for QoS-Guaranteed IoT Networks," IEEE Internet of Things Journal, 6, pp. 10902-10914, (2019).

[8] A. P. Sample, D. A. Meyer and J. R. Smith, "Analysis, Experimental Results, and Range Adaptation of Magnetically Coupled Resonators for Wireless Power Transfer," IEEE T. Ind. Electron., 58, pp. 544-554, (2011).

[9] J. Lee, Y. Lim, W. Yang, and S. Lim, "Wireless Power Transfer System Adaptive to Change in Coil Separation," IEEE T. Antenn. Propag., 62, pp. 889-897, (2014).

[10] J. Kim and J. Jeong, "Range-Adaptive Wireless Power Transfer Using Multiloop and Tunable Matching Techniques," IEEE T. Ind. Electron., 62, pp. 6233-6241, (2015).

[11] S. Zhong and X. Wang, "Energy Allocation and Utilization for Wirelessly Powered IoT Networks," in IEEE Internet of Things Journal, vol. 5, no. 4, pp. 2781-2792, Aug. 2018.

[12] S. Khairy, M. Han, L. X. Cai and Y. Cheng, "Sustainable Wireless IoT Networks With RF Energy Charging Over Wi-Fi (CoWiFi)," in IEEE Internet of Things Journal, vol. 6, no. 6, pp. 10205-10218, Dec. 2019.

[13] K. E. Jeon, J. She, J. Xue, S. Kim and S. Park, "luXbeacon—A Batteryless Beacon for Green IoT: Design, Modeling, and Field Tests," in IEEE Internet of Things Journal, vol. 6, no. 3, pp. 5001-5012, June 2019.

[14] M. Chu, X. Liao, H. Li and S. Cui, "Power Control in Energy Harvesting Multiple Access System With Reinforcement Learning," in IEEE Internet of Things Journal, vol. 6, no. 5, pp. 9175-9186, Oct. 2019.

[15] Y. Luo, L. Pu, Y. Zhao, G. Wang and M. Song, "DTER: Optimal Two-Step Dual Tunnel Energy Requesting for RF-Based Energy Harvesting System," in IEEE Internet of Things Journal, vol. 5, no. 4, pp. 2768-2780, Aug. 2018.

[16] R. Zhou, L. Wu and R. S. Cheng, "Energy-Efficiency-Oriented Charge Scheduling and Beamforming for a Two-Tier Wireless Powered Network," in IEEE Internet of Things Journal, vol. 7, no. 3, pp. 2212-2222, March 2020.

[17] Q. Zhang, W. Fang, Q. Liu, J. Wu, P. Xia and L. Yang, "Distributed Laser Charging: A Wireless Power Transfer Approach," in IEEE Internet of Things Journal, vol. 5, no. 5, pp. 3853-3864, Oct. 2018.

[18] Q. Zhang, M. Liu, X. Lin, Q. Liu, J. Wu and P. Xia, "Optimal Resonant Beam Charging for Electronic Vehicles in Internet of Intelligent Vehicles," in IEEE Internet of Things Journal, vol. 6, no. 1, pp. 6-14, Feb. 2019.

[19] W. Fang, Q. Zhang, Q. Liu, J. Wu and P. Xia, "Fair Scheduling in Resonant Beam Charging for IoT Devices," in IEEE Internet of Things Journal, vol. 6, no. 1, pp. 641-653, Feb. 2019.

[20] W. Fang, Q. Zhang, M. Liu, Q. Liu and P. Xia, "Earning Maximization With Quality of Charging Service Guarantee for IoT Devices," in IEEE Internet of Things Journal, vol. 6, no. 1, pp. 1114-1124, Feb. 2019.

[21] M. Liu, G. Wang, G. B. Giannakis, M. Xiong, Q. Liu and H. Deng, "Wireless Power Transmitter Deployment for Balancing Fairness and Charging Service Quality," in IEEE Internet of Things Journal, vol. 7, no. 3, pp. 2223-2234, March 2020.

[22] M. Xiong, M. Liu, Q. Zhang, Q. Liu, J. Wu and P. Xia, "TDMA in Adaptive Resonant Beam Charging for IoT Devices," in IEEE Internet of Things Journal, vol. 6, no. 1, pp. 867-877, Feb. 2019.

[23] Q. Zhang, W. Fang, M. Xiong, Q. Liu, J. Wu and P. Xia, "Adaptive Resonant Beam Charging for Intelligent Wireless Power Transfer," in IEEE Internet of Things Journal, vol. 6, no. 1, pp. 1160-1172, Feb. 2019.

[24] W. Wang, Q. Zhang, H. Lin, M. Liu, X. Liang and Q. Liu, "Wireless Energy Transmission Channel Modeling in Resonant Beam Charging for IoT Devices," in IEEE Internet of Things Journal, vol. 6, no. 2, pp. 3976-3986, April 2019.

[25] Q. Zhang, G. Wang, J. Chen, G. B. Giannakis and Q. Liu, "Mobile Energy Transfer in Internet of Things," in IEEE Internet of Things Journal, vol. 6, no. 5, pp. 9012-9019, Oct. 2019.

[26] G. Han, J. Wu, H. Wang, M. Guizani, J. A. Ansere and W. Zhang, "A Multicharger Cooperative Energy Provision Algorithm Based on Density Clustering in the Industrial Internet of Things," in IEEE Internet of Things Journal, vol. 6, no. 5, pp. 9165-9174, Oct. 2019.

[27] G. Han, H. Wang, H. Guan and M. Guizani, "A Mobile Charging Algorithm Based on Multi-charger Cooperation in Internet of Things," in IEEE Internet of Things Journal. doi: 10.1109/JIOT.2020.3006851

[28] L. Mo, A. Kritikakou and S. He, "Energy-Aware Multiple Mobile Chargers Coordination for Wireless Rechargeable Sensor Networks," in IEEE Internet of Things Journal, vol. 6, no. 5, pp. 8202-8214, Oct. 2019.

[29] C. Su, F. Ye, L. Wang, L. Wang, Y. Tian and Z. Han, "UAV-Assisted Wireless Charging for Energy-Constrained IoT Devices Using Dynamic Matching," in IEEE Internet of Things Journal, vol. 7, no. 6, pp. 4789-4800, June 2020.

[30] P. Wu, F. Xiao, H. Huang, C. Sha and S. Yu, "Adaptive and Extensible Energy Supply Mechanism for UAVs-aided Wireless Powered Internet of Things," in IEEE Internet of Things Journal. doi: 10.1109/JIOT.2020.3005133

[31] J. Baek, S. I. Han and Y. Han, "Optimal UAV Route in Wireless Charging Sensor Networks," in IEEE Internet of Things Journal, vol. 7, no. 2, pp. 1327-1335, Feb. 2020.

[32] W. Na, J. Park, C. Lee, K. Park, J. Kim and S. Cho, "Energy-Efficient Mobile Charging for Wireless Power Transfer in Internet of Things Networks," in IEEE Internet of Things Journal, vol. 5, no. 1, pp. 79-92, Feb. 2018.

[33] Q. Zhang, F. Li and Y. Wang, "Mobile Crowd Wireless Charging Toward Rechargeable Sensors for Internet of Things," in IEEE Internet of Things Journal, vol. 5, no. 6, pp. 5337-5347, Dec. 2018.

[34] C. Sha, D. Song and R. Malekian, "A Periodic and Distributed Energy Supplement Method based on Maximum Recharging Benefit in Sensor Networks," in IEEE Internet of Things Journal. doi: 10.1109/JIOT.2020.3020134

[35] M. Yang et al., "Dynamic Charging Scheme Problem with Actor-Critic Reinforcement Learning," in IEEE Internet of Things Journal. doi: 10.1109/JIOT.2020.3005598

[36] G. Han, X. Yang, L. Liu and W. Zhang, "A Joint Energy Replenishment and Data Collection Algorithm in Wireless Rechargeable Sensor Networks," in IEEE Internet of Things Journal, vol. 5, no. 4, pp. 2596-2604, Aug. 2018.

[37] X. Lan, Y. Zhang, L. Cai and Q. Chen, "Adaptive Transmission Design for Rechargeable Wireless Sensor Network with a Mobile Sink," in IEEE Internet of Things Journal. doi: 10.1109/JIOT.2020.3001034

[38] K. Na, H. Jang, H. Ma, and F. Bien, "Tracking Optimal Efficiency of Magnetic Resonance Wireless Power Transfer System for Biomedical Capsule Endoscopy," IEEE T. Microw. Theory, 63, pp. 295-304, (2015).

[39] S. Assawaworrarit, X. Yu and S. Fan, "Robust wireless power transfer using a nonlinear parity–time-symmetric circuit," Nature, 546, pp. 387-390, (2017).

[40] J. Park, Y. Tak, Y. Kim, Y. Kim, and S. Nam, "Investigation of Adaptive Matching Methods for Near-Field Wireless Power Transfer," IEEE T. Antenn. Propag., 59, pp. 1769-1773, (2011).

[41] W. Lee, W. Son, K. Oh, and J. Yu, "Contactless Energy Transfer Systems Using Antiparallel Resonant Loops," IEEE T. Ind. Electron., 60, pp. 350-359, (2013).

[42] Y. Zhuang, A. Chen, X. Chen, Y. Huang, H. Zhao, J. Zhou, "Range-adaptive wireless power transfer based on differential coupling using multiple bi-directional coils," IEEE Transactions on Industrial Electronics, Sept. 2019.

[43] Y. Cheng and Y. Shu, "A New Analytical Calculation of the Mutual Inductance of the Coaxial Spiral Rectangular Coils," IEEE T. Magn., 50, pp. 1-6, (2014).

[44] Y. Lyu, F. Meng, G. Yang, B. Che, Q. Wu, L. Sun, D. Erni, and J. L. Li, "A Method of Using Nonidentical Resonant Coils for Frequency Splitting Elimination in Wireless Power Transfer," IEEE T. Power Electr., 30, pp. 6097-6107, (2015).

[45] Y. Shu, X. Wei, J. Fan, R. Yang and Y. Yang, "An equivalent dipole model hybrid with artificial neural network for electromagnetic interference prediction," *IEEE Transactions on Microwave Theory and Techniques*, vol. 67, no. 5, pp. 1790-1797, May 2019.